HHS Public Access

Author manuscript

Biochemistry. Author manuscript; available in PMC 2017 January 27.

Published in final edited form as:

Biochemistry. 2015 March 10; 54(9): 1767–1777. doi:10.1021/bi501483q.

Visualizing Attack of *Escherichia coli* by the Antimicrobial Peptide Human Defensin 5

Haritha R. Chileveru, **Shion A. Lim**, **Phoom Chairatana**, **Andrew J. Wommack**, **I-Ling Chiang**, and **Elizabeth M. Nolan***

Department of Chemistry, Massachusetts Institute of Technology, Cambridge, MA 02139, USA

Abstract

Human α-defensin 5 (HD5) is a 32-residue cysteine-rich host-defense peptide that exhibits broad-spectrum antimicrobial activity and contributes to innate immunity in the human gut and other organ systems. Despite many years of investigation, its antimicrobial mechanism of action remains unclear. In this work, we report that $HD5_{ox}$, the oxidized form of this peptide that exhibits three regiospecific disulfide bonds, causes distinct morphological changes to *Escherichia coli* and other Gram-negative microbes. These morphologies include bleb formation, cellular elongation, and clumping. The blebs are up to ~1 μm wide and typically form at the site of cell division or cell poles. Studies with *E. coli* expressing cytoplasmic GFP reveal that $HD5_{ox}$ treatment causes GFP emission to localize in the bleb. To probe the cellular uptake of $HD5_{ox}$ and subsequent localization, we describe the design and characterization of a fluorophore-HD5 conjugate family. By employing these peptides, we demonstrate that fluorophore-$HD5_{ox}$ conjugates harboring the rhodamine and coumarin fluorophores enter the *E. coli* cytoplasm. On the basis of the fluorescence profiles, each of these fluorophore-$HD5_{ox}$ conjugates localizes to the site of cell division and cell poles. These studies support the notion that $HD5_{ox}$, at least in part, exerts its antibacterial activity against *E. coli* and other Gram-negative microbes in the cytoplasm.

Graphical Abstract

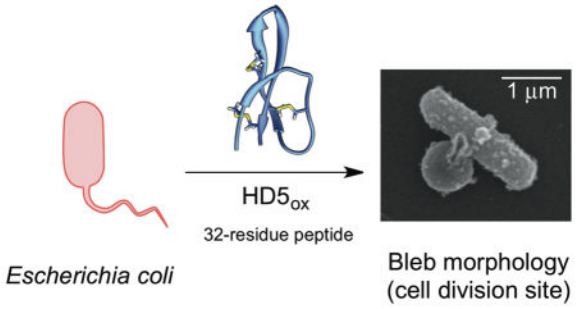

Correspondence: lnolan@mit.edu, 617-452-2495, 617-324-0505.

Supporting Information. Complete experimental methods, additional data.

Introduction

Bacterial infections and the considerable rise in antibiotic resistance in hospital and community settings pose significant problems for global health initiatives.[1,2] The dearth of new antibiotics in the drug pipeline as well as an incomplete comprehension of human innate immunity and microbial pathogenesis further confound efforts to address these challenges.[3,4] Bacterial pathogens must overcome the innate immune system, which provides first-line defense against microbial invaders, to cause human disease. Fundamental investigations that address the molecular interworking of the innate immune system are critical to further understand the host-microbe interaction and enable the development of new therapeutic strategies for infectious disease. Antimicrobial (AMPs) and/or host-defense peptides are important components of the innate immune system.[5–8] In humans, defensins[7,9] and the cathelicidin LL-37[10,11] are abundant host-defense peptides expressed and utilized by neutrophils and epithelial cells of the gastrointestinal tract, urogenital tract, airway, and skin.[12] Mammalian defensins are cysteine-rich peptides that are classified as α-, β-, and θ-defensins on the basis of regiospecific disulfide linkage patterns.[12] α-Defensins exhibit three disulfide bonds in the oxidized forms with the linkages Cys^{I}—Cys^{VI}, Cys^{II}—Cys^{IV}, Cys^{III}—Cys^{V}, and have three-stranded β-sheet structures.[7] In humans, six α-defensins are known.[7] The enteric α-defensin HD5 (Figure 1), the focus of this work, is an abundant constituent of small intestinal Paneth cell granules.[13–16] Although human defensins are established contributors to immunity, and many exhibit broad-spectrum *in vitro* antimicrobial activity, details pertaining to the physiological function of each peptide are often unclear.[12,17,18] In this work, we focus on a fundamental and outstanding question: how does HD5 kill bacteria?

How defensins kill bacteria as well as how *in vitro* antibacterial activity relates to the physiological milieu are questions of current interest and debate.[17] The oxidized α-defensins display remarkable similarity in their tertiary structure, and most characterized to date are cationic and amphipathic.[20] Moreover, defensins from various organisms have the capacity to disrupt bacterial cell membranes.[21–23] On the basis of early investigations, including seminal structural studies of HNP3,[24] a working model whereby defensins kill bacteria by non-specific membrane destabilization was presented.[21,24] Over the years, this type of model was generalized for many defensins and other antimicrobial peptides.[17] Nevertheless, defensins exhibit remarkable diversity in primary sequence, and recent studies support alternative mechanisms of action for some family members. Fungal plectasin,[25] oyster defensin,[26] and fungal copsin[27] bind lipid II and block cell wall biosynthesis. The human defensins human neutrophil peptide 1 (HNP1, α-defensin)[28] and human β-defensin 3 (HBD3)[29] are also reported to bind lipid II to varying degrees.[30] Studies of HBD3 attributed the *in vitro* antibacterial activity against *Staphylococcus aureus* to lipid II binding and subsequent cell wall lysis.[29] Recently, human β-defensin 2 (HBD2) was found to localize at septal foci of *Enterococcus faecalis* and disrupt virulence factor assembly.[31] Human α-defensin 6 (HD6) lacks antimicrobial activity *in vitro* and is proposed to serve a host-defense function by self-assembling into a web-like structure termed “nanonet” that captures bacteria in the intestinal lumen.[32,33] Taken together, these investigations highlight tremendous variation in defensin mechanism of action despite similar tertiary structures, and

demonstrate that membrane permeabilization is only one of the many factors that contribute to the *in vitro* antimicrobial activities demonstrated by this vast peptide family.

Our laboratory has initiated a research program focused on understanding the biophysical properties and biological functions of human defensins that are produced and released in the small intestine. Paneth cells,[16] located in the crypts of Lieberkühn, contain granules that store two α-defensins, HD5 and HD6, as well as other antimicrobial peptides, proteases, and a labile zinc pool of unknown function.[34,35] HD5 is the most abundant Paneth cell antimicrobial peptide,[36] and it exhibits broad-spectrum antimicrobial activity *in vitro*.[37–40] Moreover, transgenic mice expressing HD5 are more resistant to *Salmonella* challenge than wild-type mice,[41] and studies of the resident intestinal microbiota suggest that HD5 contributes to controlling its composition.[41,42] In humans suffering from ileal Crohn's disease, an inflammatory disorder of the small bowel, a deficiency in Paneth cell defensins is observed.[36] Despite these compelling observations from animal models and clinical studies, the antimicrobial mechanism of action of HD5 is not well understood.

HD5 is a 32-residue peptide with an overall charge of +4 at neutral pH (Figure 1). Over the past decade, structure-activity relationship studies of $HD5_{ox}$ evaluated the importance of quaternary structure,[4043] disulfide linkages[44,45] cationic residues,[46] the canonical α-defensin salt bridge between [Arg^6] and [Glu^{14}],[47] and chirality[48] for its *in vitro* bactericidal activity. Results from several recent studies probing interactions between $HD5_{ox}$ and *E. coli* support a model whereby (i) the Gram-negative outer membrane serves as a permeability barrier for $HD5_{ox}$[49] and (ii) the inner membrane becomes damaged as a result of $HD5_{ox}$ exposure.[44]

In this work, we utilize microscopy to investigate the attack of $HD5_{ox}$ on Gram-negative bacteria. We establish that *E. coli* treated with native $HD5_{ox}$ exhibit distinct morphologies that include clumping, cell elongation, and formation of one or more cellular blebs typically at the cell poles or division site. We demonstrate that similar morphological changes occur for other Gram-negative bacteria, including the opportunistic human pathogens *Acinetobacter baumannii* and *Pseudomonas aeruginosa*, following $HD5_{ox}$ exposure. Through the design, characterization and utilization of a fluorophore-HD5 conjugate family, we report that rhodamine- and coumarin-modified $HD5_{ox}$ enter the *E. coli* cytoplasm. Moreover, these fluorophore-HD5 conjugates preferentially localize at cell poles and cell division sites in *E. coli*, suggesting locales of a possible intracellular target.

Results and Discussion

HD5 Causes Distinct Morphological Changes in *Escherichia coli*

For morphology studies, we selected to image Gram-negative *Escherichia coli*. This microbe is a commensal microbe of the human gut as well as a pathogen of the gut and urogenital tract, and a number of studies have probed the antibacterial activity of $HD5_{ox}$ against this strain.[37,44,47] In AMA assays, the concentration of $HD5_{ox}$ required to kill *E. coli* (e.g., lethal dose 99.99% or 4-fold log reduction in CFU/mL) depends on the number of colony forming units. Our standard AMA assay for evaluating $HD5_{ox}$ activity employs mid-log phase bacteria at ≈1×10^6 CFU/mL cultured in an AMA buffer (10 mM sodium phosphate buffer pH 7.4, 1% v/v TSB without dextrose). Under these conditions, the concentration of $HD5_{ox}$

required to kill 99.99% of *E. coli* is ≈4 μM depending on the precise starting CFU/mL. Treatment of mid-log-phase *E. coli* ATCC 25922 (1×10^6 CFU/mL) with $HD5_{ox}$ (2 and 4 μM) under standard AMA assay conditions resulted in marked changes to the bacterial morphology observable by phase-contrast microscopy that included the formation of large bulges, hereafter called blebs (Figure S1). To facilitate visualizing more cells per experiment, we modified the standard AMA conditions and employed a greater number of cells (1×10^8 CFU/mL) and higher concentrations of $HD5_{ox}$ (0–80 μM). Under these conditions, $HD5_{ox}$ displays AMA, and ≈2-fold log reduction in CFU/mL is observed following treatment of the *E. coli* with 40 μM $HD5_{ox}$ (Figure S2). Moreover, the *E. coli* displayed distinct morphological changes as observed in the preliminary experiment (Figure S1). On the basis of this similarity, we employed the modified conditions with greater cell density and higher $HD5_{ox}$ concentration for further imaging experiments. The morphologies observed under these conditions included cellular elongation and the formation of blebs (Figure 2). Clumping of *E. coli* was also observed. Bacterial cells with lengths of 5 μm or greater were categorized as elongated, and cells with lengths in the 10–15 μm range were periodically observed following $HD5_{ox}$ treatment. The blebs were typically localized at the cell division sites and cell poles; however, some bacteria displayed blebs along the cell body, and some bacteria exhibited multiple blebs per cell. The blebs remained intact during the centrifugation and wash steps required for scanning electron microscopy (SEM) sample preparation. Indeed, the blebs as well as what appeared to be outer membrane vesicles (Figure S3) and cellular debris (*vide infra*) were markedly apparent in SEM images (Figure 2).

Neither blebs nor elongation were observed for untreated cells, and the number of cells exhibiting these morphological changes increased with increasing $HD5_{ox}$ (0–80 μM) (Figure 3). Following exposure to 20 μM $HD5_{ox}$, ~17% of cells exhibited blebs and 2% were elongated (n = 212 cells). These values increased to ~30% and ≥4% at ≥40 μM $HD5_{ox}$, respectively (n = 203 cells). We performed time-course experiments where *E. coli* were exposed to 20 μM $HD5_{ox}$ on the microscope stage and imaged over time (~2 h). Many of the treated cells displayed blebs, and the blebbing cells did not lyse over the course of this experiment (Figure S4). Propidium iodide (PI) uptake was therefore employed to evaluate the viability of $HD5_{ox}$-treated cells, and the cells exhibiting blebs were labeled with PI, which indicated that bleb formation correlated with cell death (Figure S5). The morphological changes observed for *E. coli* ATCC 25922 were comparable to those we recently reported for *E. coli* K-12 and select mutants from the Keio Collection.[50]

The susceptibility of *E. coli* to $HD5_{ox}$ depends on the growth phase, and stationary phase cultures exhibit resistance to $HD5_{ox}$ relative to mid-log phase cultures as observed for other defensins.[21,38] In this work, treatment of mid-log phase *E. coli* with 4 μM $HD5_{ox}$ resulted in an ~4-fold log-reduction in CFU/mL whereas only ~2-fold log-reduction was observed for stationary phase *E. coli* (Figure S6). In agreement with this trend, fewer morphological changes were observed for stationary phase cells treated with $HD5_{ox}$ (Figures 3, S6). Taken together, the microscopy and antimicrobial activity assays with $HD5_{ox}$ and *E. coli* provided a correlation between bacterial susceptibility and altered cellular morphology.

Treatment of *E. coli* with Other AMPs Does Not Result in the Bleb Morphology

We questioned whether other antimicrobial peptides confer the same morphological changes observed for $HD5_{ox}$ under the experimental conditions used in this work. Prior biophysical studies proposed the ability of the murine Paneth cell defensin cryptdin-4 to induce negative curvature on bacterial membranes, resulting in structures called blebs or pores.[51] To visualize the effect of cryptdin-4 on *E. coli* morphology, we first obtained cryptdin-4 by overexpression in *E. coli*, and confirmed its antimicrobial activity (Supporting Information, Figure S9). The *E. coli* treated with cryptdin-4 (20 μM) did not form large blebs as observed for $HD5_{ox}$ (Figure 4). Likewise, *E. coli* did not exhibit blebs following exposure to the pore-forming antimicrobial peptide melittin[52] (20 μM), the LPS-associated membrane-destabilizing peptide colistin[53] (20 μM), or the pore-forming antimicrobial peptide human LL-37[54] (20 μM) (Figure 4). The bacteria treated with LL-37 were somewhat elongated relative to the untreated control cells. Small membrane protrusions (<100nm wide) and surface roughness observed for bacteria treated with AMPs such as magainin 2[55] and Bac8c[56] have been described as blebs. To the best of our knowledge, larger blebs (~1-μm wide), formed preferentially at poles and cell division sites as observed for $HD5_{ox}$, have not been reported for a human host-defense peptide. The most similar bleb morphologies we identified in the literature are the bulges that result from β-lactam treatment.[57] Moreover, a knockout mutant of elyC,[58] an inner-membrane protein involved in peptidoglycan synthesis from the Keio Collection, and some Tol-Pal mutants of *Caulobacter crescentus*,[59] are reported to display large blebs.

On the basis of this modest AMP screen, we concluded that $HD5_{ox}$ affects *E. coli* differently than the other AMPs considered in this work, including the murine α-defensin cryptdin-4. Although morphology comparisons alone do not provide detailed insight into antibiotic mechanisms, our imaging results suggest that the mechanism of action of $HD5_{ox}$ against *E. coli* cannot be explained fully by membrane permeabilization.

$HD5_{ox}$ Causes Similar Morphological Changes in Other Gram-negative Organisms

$HD5_{ox}$ exhibits broad-spectrum antibacterial activity[37,38,40] and whether its mechanism of action is general or strain-specific remains unclear. Several structure/activity relationship studies indicated that $HD5_{ox}$ operates by different mechanisms for Gram-negative and –positive organisms, but these studies were limited to comparisons between *E. coli* and *Staphylococcus aureus*.[44,45,48] To delineate whether $HD5_{ox}$ perturbs the morphologies of other Gram-negative strains, four human pathogens, *Acinetobacter baumannii* 17978, *Klebsiella pneumoniae* 13883, *Pseudomonas aeruginosa* PAO1, and *E. coli* CFT073, were evaluated along with the laboratory strain *E. coli* K-12 (Figure 5). As for non-pathogenic *E. coli* ATCC 25922 and K-12, bleb formation, elongation, and clumping were observed for the pathogenic strains. We previously reported that *A. baumannii* exhibits relatively high sensitivity to $HD5_{ox}$.40 In accordance with this observation, *A. baumannii* displayed blebs at 10 μM $HD5_{ox}$ (Figure S8). *P. aeruginosa* is less susceptible to $HD5_{ox}$ killing,[40] and blebs were only observed with 40 μM of $HD5_{ox}$ (Figure S8).

Morphological Changes are Attenuated by Salt and Divalent Metal Ions

The *in vitro* antimicrobial activity of many defensins is attenuated by the presence of salt and divalent cations.[60] This phenomenon is commonly attributed to a disruption of electrostatic interactions between the cationic defensin and anionic bacterial cell membrane.[17] Like many defensins, the antibacterial activity of $HD5_{ox}$ is attenuated by millimolar concentrations of sodium chloride.[38] We observed that NaCl prevents bleb formation and other morphological changes associated with $HD5_{ox}$ activity. Indeed, *E. coli* co-treated with $HD5_{ox}$ (40 μM) and NaCl (200 mM) displayed a smooth morphology similar to that of the untreated control (Figure S7). The divalent cations Ca(II), Mg(II) and Zn(II) also blocked $HD5_{ox}$ activity (Figure S5). This effect was most potent for Zn(II) where a 2:1 Zn(II):$HD5_{ox}$ molar ratio resulted in a loss of antibacterial activity and $HD5_{ox}$- associated morphologies. This observation is of broad interest because the Paneth cell granules, which harbor HD5, also contain a labile zinc pool of unknown function.[34]

Disulfide Bonds Are Necessary for the Bleb Morphology

The canonical α-defensin disulfide array provides a three-stranded β-sheet fold to each $HD5_{ox}$ monomer. This compact structure orients the positively charged residues on one face of the peptide and the hydrophobic residues on the opposite, rendering HD5 amphipathic.[19] To investigate the structural requirements for $HD5_{ox}$ activity, we evaluated the consequences of treating *E. coli* with three HD5 derivatives, HD5-TE, HD5-CD, and $HD5[E21S]_{ox}$, selected to probe the disulfide array as well as quaternary structure. HD5-TE is a linear disulfide-null analogue where the six cysteines are carboxymethylated with 2-iodoacetamide.[61] Defensins have the propensity to self-associate, and in prior work we reported that $HD5_{ox}$ forms tetramers at neutral pH.[19] HD5-CD is a C_2-symmetric covalent dimer of $HD5_{ox}$ with a cationic surface that results from intermolecular disulfide exchange between the Cys^5–Cys^{20} disulfide bonds (canonical Cys^{II}—Cys^{IV}) of two HD5 monomers.[40] We also prepared and characterized $HD5[E21S]_{ox}$, a new $HD5_{ox}$ mutant that forms a non-covalent dimer, but not a tetramer, at neutral pH (Supporting Information, Table S3, Figure S23).

E. coli treated with HD5-CD or $HD5[E21S]_{ox}$ were indistinguishable from those treated with $HD5_{ox}$ (Figure 6), in agreement with antimicrobial activity assays where both $HD5[E21S]_{ox}$ and HD5-CD killed *E. coli* (Figure S10). In contrast, the antimicrobial activity of linear and unstructured HD5-TE against *E. coli* was attenuated (2-fold log reduction of CFU/mL at 16 μM) relative to $HD5_{ox}$. HD5-TE did not cause bleb formation (Figure 6); however, SEM revealed that the cells treated with HD5-TE were corrugated and frequently elongated (Figure S11). These results highlight the importance of cysteine residues housed in disulfide linkages in the overall antimicrobial activity of HD5 and the induced morphological changes.

Blebs Accumulate the Cytoplasmic Contents

The blebs observed in this work are reminiscent of the cellular morphologies that result from treatment of *E. coli* with β-lactams, and *E. coli* strains expressing GFP have proven to be useful in imaging studies of β-lactam action.[57,62] Guided by this work, we investigated the contents as well as time-dependent formation of the blebs by employing an *E. coli* strain that

expresses cytoplasmic GFP (*E. coli* cyto-GFP). Mid-log phase *E. coli* cyto-GFP formed blebs following exposure to $HD5_{ox}$. The blebs displayed GFP emission, and the GFP emission from the cell body was markedly reduced, suggesting that cytoplasmic contents localized to the blebs (Figure 7). Some additional phenotypes were observed for dividing cells. In several instances where a dividing cell exhibited a bleb at the cell division site, the GFP localization differed between the daughter cells (Figure S12). Moreover, for cells with blebs at the cell division site, the GFP intensity in the region between the two daughter cells was relatively weak, indicating that the presence of a membrane at the division plane. In agreement with this observation, labeling $HD5_{ox}$-treated *E. coli* ATCC 25922 with the membrane-binding dye FM4-64 confirmed the presence of this membrane (Figure S13).

Cell viability, as observed by PI uptake, was inversely correlated to the overall GFP fluorescence intensity of the bacteria (Figure S12). When *E. coli* cyto-GFP (1×10^8 CFU/mL) were treated with $HD5_{ox}$ (20 μM) and subsequently stained as a result of PI uptake (5 μg/mL), the cells with brighter GFP emission and fewer morphological defects exhibited less PI labeling relative to cells that were affected by $HD5_{ox}$.

In agreement with studies using *E. coli* ATCC 25922 (Figure 3), negligible changes in morphology and GFP localization were observed for $HD5_{ox}$-treated *E. coli* cyto-GFP in stationary phase. To obtain quantitative comparisons, the GFP intensity and morphological changes for both mid-log phase and stationary-phase *E. coli* cyto-GFP were analyzed (Figure S15). The mean cell length for the mid-log phase cells increased from 2.8 ± 0.8 μm to 3.4 ± 1.0 μm (Student's t-test: t-value = 6.32, t-probability = <0.0001) with increasing $HD5_{ox}$ (0–80 μM), and the mean GFP fluorescence intensity decreased accordingly (155 ± 48 units to 93 ± 47 units). Only minor changes in both cell lengths (3.0 ± 0.8 μm to 2.9 ± 0.7 μm) (Student's t-test: t-value = 1.97, t-probability = 0.049) and mean intensities (112 ± 38 units to 139 ± 53 units) were found when stationary phase cells were treated with $HD5_{ox}$.

To obtain temporal information on bleb formation and GFP redistribution, we performed time-course experiments where *E. coli* cyto-GFP were treated with $HD5_{ox}$ on the microscope stage and collected images over a 2 h period (Figure 8). The replication time for *E. coli* in the standard AMA buffer (10 mM sodium phosphate buffer, pH 7.4, 1% v/v TSB without dextrose) on a MatTek plate ranged from 90–120 min at 37 °C. These cultures were unsynchronized, and bleb formation occurred at different time points depending on the cell. Blebs were observed immediately for some cells whereas others formed blebs after ~30 min exposure to $HD5_{ox}$. After the appearance of one or more blebs, GFP intensity in the cell body diminished in all cases observed. Although dividing *E. coli* were observed for untreated cells (Figure 8, top panels), cells that were affected by $HD5_{ox}$ no longer divided (Figure 8, bottom panels).

Membrane Composition of the Blebs and Observation of Outer Membrane Vesicles

The composition of the membrane surrounding the blebs of $HD5_{ox}$-treated *E. coli* was investigated by fluorescence imaging of an *E. coli* strain harboring a plasmid encoding periplasmic GFP (*E. coli* peri-GFP) as well as transmission electron microscopy (TEM) of *E. coli* ATCC 25922. These studies afforded several phenotypes and suggested that two

different types of blebs form (Figure S16). Some cells exhibited a ring of GFP emission around the blebs, which indicated that both the outer and inner membranes surrounded the bleb and were in tact. Other cells presented uniform GFP emission throughout the bleb. Possible explanations for this phenotype include (i) only the outer membrane surrounded the blebs or (ii) the inner membrane surrounded the bleb, but was damaged and leaked the periplasmic contents into the bleb. TEM imaging revealed that the blebs are membrane bound; however, it was difficult to confirm whether one or both membranes surround each bleb (Figure S17).

TEM also revealed profound changes to the *E. coli* cell surface upon $HD5_{ox}$ treatment, including vesicles surrounded by a membrane that often clustered in chain-like arrangements (Figure S17F). During phase-contrast imaging of $HD5_{ox}$-treated bacteria, we frequently observed surface-appended structures resembling debris. We attribute these structures, at least in part, to outer membrane vesicle (OMVs) on the basis of TEM and SEM studies (Figure S3). Formation of OMVs (~20–200 nm wide) is an important bacterial stress response pathway, and OMVs contribute to pathogenesis.[63] Thus, we speculate that *E. coli* may attempt to evade $HD5_{ox}$ by generating and shedding OMVs, along with $HD5_{ox}$, into the extracellular space.

Design and Synthesis of Fluorophore-HD5 Conjugates for Visualizing Peptide Localization

To probe the cellular localization of $HD5_{ox}$, we designed, prepared and characterized a seven-member family of fluorophore-HD5 conjugates (Figure 9A, B, Figure S16 and Supporting Information). Because addition of a fluorophore constitutes a substantial modification to a 32-residue peptide that may perturb the function and cellular localization of the native peptide, we evaluated the behavior of fluorophore-HD5 conjugates harboring different fluorophores as well as peptides harboring rhodamine attached to different positions (Table S1). First, we modified the N-terminus of HD5 with three different fluorophores that afford variable photophysical properties as well as overall charge. We selected coumarin 343 (C), fluorescein (FL), and rhodamine B 4-(3-carboxypropionyl)piperazine amide (R)[64] as fluorophores to achieve emission properties spanning the ~490- to ~590-nm range. Moreover, we reasoned that the overall charge of the fluorophore-modified peptide may influence its antimicrobial activity. Coumarin 343 is neutral following coupling to an α-amino group, fluorescein is anionic, and rhodamine B is cationic. This selection allowed us to probe the effect of fluorophore charge on the antimicrobial activity and cellular localization of fluorophore-$HD5_{ox}$ conjugates. We prepared R-HD5[R9K] and R-HD5[R13K] to evaluate the consequences of fluorophore positioning within the peptide sequence. We selected these positions because (i) prior structure-activity relationship studies reported that R9K and R13K mutants retained some antimicrobial activity,[46,] and (ii) the X-ray crystal structure (PDB: 1ZMP)[20] and NMR solution structure (PDB: 2LXZ)[19] of $HD5_{ox}$ revealed that side-chains of R9 and R13 are solvent exposed and directed away from the dimer interface of native $HD5_{ox}$.

The syntheses of the fluorophore-HD5 conjugates were achieved using Fmoc-based solid-phase peptide synthesis (SPPS) as described previously.[40] Analytical and photophysical characterization of the peptides is detailed in the Supporting Information (Tables S1 and S2,

Figure S18). To determine whether the absence of disulfide bonds influences cellular localization, two disulfide-null mutants, RHD5-TE and FL-HD5-TE, were synthesized by capping the cysteines of the reduced peptides, R-$HD5_{red}$ and FL-$HD5_{red}$, with 2-iodoacetamide (Supporting Information).

Fluorophore Modifications Influence the Antibacterial Activity of HD5

To assess the impact of fluorophore modification on $HD5_{ox}$ function, the AMAs of the conjugates against *E. coli* ATCC 25922 (1×10^6 CFU/mL) were first evaluated and compared to that of native $HD5_{ox}$ (Figures 9C, S18C). Fluorophore modification attenuated the cell killing ability of $HD5_{ox}$ to varying degrees. The antibacterial activity (reported as the lethal dose for 99.99% killing, $LD_{99.99}$) of $HD5_{ox}$ and the analogues harboring N-terminal fluorophores followed a trend where $HD5_{ox}$ (8 μM) > R-$HD5_{ox}$ (16 μM) > C-$HD5_{ox}$ (28 μM) > FL-$HD5_{ox}$ (>128 μM) (Figure 9C). This trend suggests that the charge of the fluorophore may influence antimicrobial activity. Additional factors, such as the physiochemical properties of the fluorophores and linkers (e.g. succinic acid spacer for R-$HD5_{ox}$) may also contribute to such changes in the antimicrobial activity of modified $HD5_{ox}$. R-HD5[R9K] and R-HD5[R13K] were active against *E. coli* and the linear derivatives were less active compared to their respective folded peptides, as expected (Figure S18C).

$HD5_{ox}$ Enters the *E. coli* Cytoplasm and Localizes to the Cell Poles and Division Site

On the basis of the AMA assay results described above, we first investigated the cellular localization of R-$HD5_{ox}$. We observed $HD5_{ox}$-like morphological changes, including bleb formation, for *E. coli* ATCC 25922 (Figure 10) and *E. coli* CFT073 (Figure S19). Intracellular fluorescence was also observed. Co-labeling studies with the membrane-binding dye FM1-43 revealed that the FM1-43 emission profile enclosed a significant portion of the R-$HD5_{ox}$ fluorescence intensity profile (Figures 10,11), which indicates that the peptide penetrated the outer and inner membranes and entered the cytoplasm. In most of the cells examined by fluorescence microscopy, the rhodamine emission was most intense at the poles and division plane. This type of labeling pattern was not observed for R-HD5-TE or rhodamine-modified LL-37 (Figure S20), both of which provided uniform cytoplasmic fluorescence.

When *E. coli* were treated with R-$HD5_{ox}$ under conditions that result in attenuated $HD5_{ox}$ activity (*vide supra*), different labeling patterns were observed. For instance, the presence of NaCl (200 mM) resulted in rhodamine emission only at the cell surface, indicating that R-$HD5_{ox}$ did not enter *E. coli* (Figure S22). Stationary-phase *E. coli* treated with R-$HD5_{ox}$ exhibited diminished intracellular fluorescence relative to mid-log phase cells (Figure S22). Taken together, these observations support a model whereby $HD5_{ox}$ must overcome the outer membrane permeability barrier and enter the cytosol to exert its full capacity to kill bacteria.

Co-incubation of *E. coli* with a 1:1 molar ratio of rhodamine B and $HD5_{ox}$ resulted in uniform cytoplasmic staining whereas treatment of *E. coli* with rhodamine B alone resulted in negligible cellular fluorescence (Figure S21). This result suggested that $HD5_{ox}$ treatment

allowed for rhodamine B entry as a result of membrane permeabilization, and confirmed that covalent attachment of rhodamine to $HD5_{ox}$ is essential for observing fluorescence localized to the cell poles and division site. The R-HD5[R13K]$_{ox}$ conjugate provided a similar labeling pattern as R-$HD5_{ox}$ and thereby indicated that localization of the rhodamine-$HD5_{ox}$ conjugate is not an artifact resulting from a particular site of rhodamine attachment (Figure S20). Moreover, C-$HD5_{ox}$ preferentially labeled the cell poles and cell division sites, and co-labeling with the membrane-binding dye FM 4-64 confirmed its cytoplasmic localization (Figures 10,11). The fact that the same labeling pattern was observed for $HD5_{ox}$ modified with either rhodamine or coumarin, taken with these modified peptides causing the same morphological changes as observed for unmodified $HD5_{ox}$, provides a strong indication that the localization is a result of $HD5_{ox}$, and not the fluorophore.

It should be noted that FL-$HD5_{ox}$, which provided no *in vitro* antibacterial activity against *E. coli* at the highest concentration evaluated (128 μM), did not enter *E. coli*. Rather, the peptide afforded a punctate labeling pattern on and around the bacterial surface (Figures 10,11). We attribute this phenomenon to the overall negative charge of the fluorescein moiety.

The fluorescence imaging studies of $HD5_{ox}$ may be considered in the context of other AMPs that have been examined by similar approaches to probe uptake and mechanism of action. For instance, fluorescence microscopy revealed that buforin II entered the bacterial cytoplasm without permeabilizing the inner membrane.[65] A rhodamine derivative of the only human cathelicidin, LL-37, attacked septating *E. coli* more readily than non-septating cells and permeabilized the bacteria via a carpet-model of membrane destabilization.[66,67] A fluorophore-labeled lantibiotic was shown to interact with lipid II of *B. subtilis* 168.[68] Recent imaging studies of Cy3-derivaitzed HBD2 indicated that HBD2 preferentially localizes to the nascent poles and cell division site of *Enterococcus faecalis*.[31] This focal labeling pattern was attributed to the binding of the HBD2 to anionic lipids in these regions. The cell poles and division site of *E. coli* are also enriched in negatively charged phospholipids that include cardiolipin and phosphatidylglycerol.[69] Whether $HD5_{ox}$ also binds to anionic lipids at the cell poles of *E. coli* and/or another target in these locales is currently unknown and a topic for future investigation.

Summary and Outlook

In this study, we defined how the antimicrobial peptide $HD5_{ox}$ affects the morphology of *E. coli* and other Gram-negative bacteria. We established that $HD5_{ox}$ causes distinct morphological changes to *E. coli* as well as *K. pneumoniae*, *A. baumannii*, and *P. aeruginosa* that include bleb formation, cellular clumping, and elongation. We also demonstrated that other AMPs, including human LL-37 and murine α-defensin cryptdin-4, do not cause such morphologies. Taken together, these observations indicate that $HD5_{ox}$ kills *E. coli* by a different mechanism than the other peptides examined in this work. Our results highlight the importance of treating host-defense peptides individually, and not generalizing cell-killing mechanisms.

Defensins are often described as membrane-disrupting peptides. Our prior investigations indicate that $HD5_{ox}$ traverses the outer membrane and subsequently damages the inner membrane of *E. coli*.[44,50] In this work, the insights gained from utilizing fluorophore-$HD5_{ox}$ conjugates modified with rhodamine or coumarin support a model that $HD5_{ox}$ enters the *E. coli* cytoplasm. Because the cytoplasm is a reducing environment, intracellular reduction of the $HD5_{ox}$ disulfide array to liberate free cysteine residues may occur. Deciphering whether such redox chemistry contributes to altered cellular morphologies and cell killing warrants exploration. The cytoplasmic localization also supports the possibility that $HD5_{ox}$ (or the reduced form) has an as-yet undiscovered intracellular target. Indeed, the intracellular staining pattern at the cell poles and cell division site routinely observed for *E. coli* treated with R/C-$HD5_{ox}$ suggests the locale of a possible target. On the basis of this localization, coupled with the elongation phenotype observed for *E. coli* and other Gram-negative microbes, we reason that $HD5_{ox}$ may exert antimicrobial activity by affecting cell division. Efforts are underway to further investigate this notion.

Materials and Methods

Complete Materials and Methods are provided as Supporting Information.

Supplementary Material

Refer to Web version on PubMed Central for supplementary material.

Acknowledgments

We thank Prof. Daniel Kahne for insightful discussions; Prof. Bradley Pentelute and members of the Pentelute Lab for expertise in flow-based peptide synthesis; Yunfei Zhang for performing initial Zn(II) experiments; Jill Tomaras for microbiology assistance; Nicki Watson at of the Whitehead Institute for Biomedical Research for preparing the TEM samples and imaging; Prof. K. Ribbeck for providing the *E. coli* cyto-GFP strain.

Funding. This work was supported by the NIH (Grant DP2OD007045 from the Office of the Director). HRC was a recipient of a 2014 Richard R. Schrock summer graduate fellowship; PC is a recipient of a Royal Thai Government Fellowship; SAL and ILC received research funding from the MIT UROP Program. The Biophysical Instrumentation Facility for the Study of Complex Macromolecular Systems (NSF-007031) is gratefully acknowledged. The Institute for Soldier Nanotechnologies is supported in part by the U. S. Army Research Laboratory and the U. S. Army Research Office through the Institute for Soldier Nanotechnologies, under contract number W911NF-13-D-0001.

Abbreviations

AMA	Antimicrobial activity
C	Coumarin 343
CFU	Colony forming unit
Crp-4	Cryptdin-4 (a murine α-defensin)
FL	5(6)-Carboxyfluorescein
FM1-43	(*N*-(3-Triethylammoniumpropyl)-4-(4-(dibutylamino) styryl)pyridiniumdibromide)

FM4-64	(*N*-(3-Triethylammoniumpropyl)-4-(6-(4-(diethylamino)phenyl)hexatrienyl)pyridiniumdibromide)
HD5	Human α-defensin 5
$HD5_{red}$	Reduced form of human α-defensin 5
$HD5_{ox}$	Oxidized form of human α-defensin 5
HD5-TE	Linear form of human α-defensin 5 (iodoacetamide-capped)
HD5-CD	Human α-defensin 5 covalent dimer
PI	Propidium iodide
R	Rhodamine B 4-(3-carboxypropionyl)piperazine amide
SEM	Scanning electron microscopy
TEM	Transmission electron microscopy
TSB	Trypticase soy broth

References

1. WHO. Antimicrobial resistance: global report on surveillance. 2014.
2. Davies J, Davies D. Origins and evolution of antibiotic resistance. Microbiol Mol Biol Rev. 2010; 74:417–433. [PubMed: 20805405]
3. Fischbach MA, Walsh CT. Antibiotics for emerging pathogens. Science. 2009; 325:1089–1093. [PubMed: 19713519]
4. Lewis K. Platforms for antibiotic discovery. Nat Rev Drug Discov. 2013; 12:371–387. [PubMed: 23629505]
5. Jenssen H, Hamill P, Hancock REW. Peptide antimicrobial agents. Clin Microbiol Rev. 2006; 19:491–511. [PubMed: 16847082]
6. Choi KY, Chow LNY, Mookherjee N. Cationic host defence peptides: multifaceted role in immune modulation and inflammation. J Innate Immun. 2012; 4:361–370. [PubMed: 22739631]
7. Lehrer RI, Lu W. α-Defensins in human innate immunity. Immunol Rev. 2012; 245:84–112. [PubMed: 22168415]
8. Cruz J, Ortiz C, Guzmán F, Fernández-Lafuente R, Torres R. Antimicrobial peptides: promising compounds against pathogenic microorganisms. Curr Med Chem. 2014; 21:2299–2321. [PubMed: 24533812]
9. Ganz T. Defensins: antimicrobial peptides of innate immunity. Nat Rev Immunol. 2003; 3:710–720. [PubMed: 12949495]
10. Ramanathan B, Davis EG, Ross CR, Blecha F. Cathelicidins: microbicidal activity, mechanisms of action, and roles in innate immunity. Microbes Infect. 2002; 4:361–372. [PubMed: 11909747]
11. Gennaro R, Zanetti M. Structural features and biological activities of the cathelicidin-derived antimicrobial peptides. Biopolymers. 2000; 55:31–49. [PubMed: 10931440]
12. Selsted ME, Ouellette AJ. Mammalian defensins in the antimicrobial immune response. Nat Immunol. 2005; 6:551–557. [PubMed: 15908936]
13. Jones DE, Bevins CL. Paneth cells of the human small intestine express an antimicrobial peptide gene. J Biol Chem. 1992; 267:23216–23225. [PubMed: 1429669]
14. Porter EM, Liu L, Oren A, Anton PA, Ganz T. Localization of human intestinal defensin 5 in Paneth cell granules. Infect Immun. 1997; 65:2389–2395. [PubMed: 9169779]

15. Ayabe T, Ashida T, Kohgo Y, Kono T. The role of Paneth cells and their antimicrobial peptides in innate host defense. Trends Microbiol. 2004; 12:394–398. [PubMed: 15276616]
16. Clevers HC, Bevins CL. Paneth cells: maestros of the small intestinal crypts. Annu Rev Physiol. 2013; 75:289–311. [PubMed: 23398152]
17. Brogden KA. Antimicrobial peptides: pore formers or metabolic inhibitors in bacteria? Nat Rev Microbiol. 2005; 3:238–250. [PubMed: 15703760]
18. Hilchie AL, Wuerth K, Hancock REW. Immune modulation by multifaceted cationic host defense (antimicrobial) peptides. Nat Chem Biol. 2013; 9:761–768. [PubMed: 24231617]
19. Wommack AJ, Robson SA, Wanniarachchi YA, Wan A, Turner CJ, Wagner G, Nolan EM. NMR solution structure and condition-dependent oligomerization of the antimicrobial peptide human defensin 5. Biochemistry. 2012; 51:9624–9637. [PubMed: 23163963]
20. Szyk A, Wu Z, Tucker K, Yang D, Lu W, Lubkowski J. Crystal structures of human alpha-defensins HNP4, HD5, and HD6. Protein Sci. 2006; 15:2749–2760. [PubMed: 17088326]
21. Lehrer RI, Barton A, Daher KA, Harwig SS, Ganz T, Selsted ME. Interaction of human defensins with *Escherichia coli* Mechanism of bactericidal activity. J Clin Invet. 1989; 84:553–561.
22. Zasloff M. Antimicrobial peptides of multicellular organisms. Nature. 2002; 415:389–395. [PubMed: 11807545]
23. Figueredo SM, Weeks CS, Young SK, Ouellette AJ. Anionic amino acids near the pro-alpha-defensin N terminus mediate inhibition of bactericidal activity in mouse pro-cryptdin-4. J Biol Chem. 2009; 284:6826–6831. [PubMed: 19106102]
24. Hill CP, Yee J, Selsted ME, Eisenberg D. Crystal structure of defensin HNP-3, an amphiphilic dimer: mechanisms of membrane permeabilization. Science. 1991; 251:1481–1485. [PubMed: 2006422]
25. Schneider T, Kruse T, Wimmer R, Wiedemann I, Sass V, Pag U, Jansen A, Nielsen AK, Mygind PH, Raventós DS, Neve S, Ravn B, Bonvin AMJJ, De Maria L, Andersen AS, Gammelgaard LK, Sahl HG, Kristensen HH. Plectasin, a fungal defensin, targets the bacterial cell wall precursor Lipid II. Science. 2010; 328:1168–1172. [PubMed: 20508130]
26. Schmitt P, Wilmes M, Pugnière M, Aumelas A, Bachère E, Sahl HG, Schneider T, Destoumieux-Garzón D. Insight into invertebrate defensin mechanism of action: oyster defensins inhibit peptidoglycan biosynthesis by binding to lipid II. J Biol Chem. 2010; 285:29208–29216. [PubMed: 20605792]
27. Essig A, Hofmann D, Münch D, Gayathri S, Künzler M, Kallio PT, Sahl HG, Wider G, Schneider T, Aebi M. Copsin, a novel peptide-based fungal antibiotic interfering with the peptidoglycan synthesis. J Biol Chem. 2014; 289:34953–34964. [PubMed: 25342741]
28. De Leeuw E, Li C, Zeng P, Li C, Diepeveen-de Buin M, Lu WY, Breukink E, Lu W. Functional interaction of human neutrophil peptide-1 with the cell wall precursor lipid II. FEBS Lett. 2010; 584:1543–1548. [PubMed: 20214904]
29. Sass V, Schneider T, Wilmes M, Körner C, Tossi A, Novikova N, Shamova O, Sahl HG. Human beta-defensin 3 inhibits cell wall biosynthesis in *Staphylococci*. Infect Immun. 2010; 78:2793–2800. [PubMed: 20385753]
30. Wilmes M, Sahl HG. Defensin-based anti-infective strategies. Int J Med Microbiol. 2014; 304:93–99. [PubMed: 24119539]
31. Kandaswamy K, Liew TH, Wang CY, Huston-Warren E, Meyer-Hoffert U, Hultenby K, Schröder JM, Caparon MG, Normark S, Henriques-Normark B, Hultgren SJ, Kline KA. Focal targeting by human β-defensin 2 disrupts localized virulence factor assembly sites in *Enterococcus faecalis*. Proc Natl Acad Sci U S A. 2013; 110:20230–20235. [PubMed: 24191013]
32. Chu H, Pazgier M, Jung G, Nuccio SP, Castillo PA, de Jong MF, Winter MG, Winter SE, Wehkamp J, Shen B, Salzman NH, Underwood MA, Tsolis RM, Young GM, Lu W, Lehrer RI, Bäumler AJ, Bevins CL. Human α-defensin 6 promotes mucosal innate immunity through self-assembled peptide nanonets. Science. 2012; 337:477–481. [PubMed: 22722251]
33. Chairatana P, Nolan EM. Molecular basis for self-assembly of a human host-defense Peptide that entraps bacterial pathogens. J Am Chem Soc. 2014; 136:13267–13276. [PubMed: 25158166]

34. Giblin LJ, Chang CJ, Bentley AF, Frederickson C, Lippard SJ, Frederickson CJ. Zinc-secreting Paneth cells studied by ZP fluorescence. J Histochem Cytochem. 2006; 54:311–316. [PubMed: 16260591]
35. Dinsdale D. Ultrastructural localization of zinc and calcium within the granules of rat Paneth cells. J Histochem Cytochem. 1984; 32:139–145. [PubMed: 6693753]
36. Wehkamp J, Salzman NH, Porter E, Nuding S, Weichenthal M, Petras RE, Shen B, Schaeffeler E, Schwab M, Linzmeier R, Feathers RW, Chu H, Lima H, Fellermann K, Ganz T, Stange EF, Bevins CL. Reduced Paneth cell alpha-defensins in ileal Crohn's disease. Proc Natl Acad Sci U S A. 2005; 102:18129–18134. [PubMed: 16330776]
37. Ericksen B, Wu Z, Lu W, Lehrer RI. Antibacterial activity and specificity of the six human {alpha}-defensins. Antimicrob Agents Chemother. 2005; 49:269–275. [PubMed: 15616305]
38. Porter EM, van Dam E, Valore EV, Ganz T. Broad-spectrum antimicrobial activity of human intestinal defensin 5. Infect Immun. 1997; 65:2396–2401. [PubMed: 9169780]
39. Nuding S, Zabel LT, Enders C, Porter E, Fellermann K, Wehkamp J, Mueller HAG, Stange EF. Antibacterial activity of human defensins on anaerobic intestinal bacterial species: a major role of HBD-3. Microbes Infect. 2009; 11:384–393. [PubMed: 19397883]
40. Wommack AJ, Ziarek JJ, Tomaras J, Chileveru HR, Zhang Y, Wagner G, Nolan EM. Discovery and characterization of a disulfide-locked C_2-symmetric defensin Peptide. J Am Chem Soc. 2014; 136:13494–13497. [PubMed: 25181039]
41. Salzman NH, Ghosh D, Huttner KM, Paterson Y, Bevins CL. Protection against enteric salmonellosis in transgenic mice expressing a human intestinal defensin. Nature. 2003; 422:522–526. [PubMed: 12660734]
42. Salzman NH, Hung K, Haribhai D, Chu H, Karlsson-Sjöberg J, Amir E, Teggatz P, Barman M, Hayward M, Eastwood D, Stoel M, Zhou Y, Sodergren E, Weinstock GM, Bevins CL, Williams CB, Bos NA. Enteric defensins are essential regulators of intestinal microbial ecology. Nat Immunol. 2010; 11:76–83. [PubMed: 19855381]
43. Rajabi M, Ericksen B, Wu X, de Leeuw E, Zhao L, Pazgier M, Lu W. Functional determinants of human enteric α-defensin HD5: crucial role for hydrophobicity at dimer interface. J Biol Chem. 2012; 287:21615–21627. [PubMed: 22573326]
44. Wanniarachchi YA, Kaczmarek P, Wan A, Nolan EM. Human defensin 5 disulfide array mutants: disulfide bond deletion attenuates antibacterial activity against *Staphylococcus aureus*. Biochemistry. 2011; 50:8005–8017. [PubMed: 21861459]
45. De Leeuw E, Burks SR, Li X, Kao JPY, Lu W. Structure-dependent functional properties of human defensin 5. FEBS Lett. 2007; 581:515–520. [PubMed: 17250830]
46. De Leeuw E, Rajabi M, Zou G, Pazgier M, Lu W. Selective arginines are important for the antibacterial activity and host cell interaction of human alpha-defensin 5. FEBS Lett. 2009; 583:2507–2512. [PubMed: 19589339]
47. Rajabi M, de Leeuw E, Pazgier M, Li J, Lubkowski J, Lu W. The conserved salt bridge in human alpha-defensin 5 is required for its precursor processing and proteolytic stability. J Biol Chem. 2008; 283:21509–21518. [PubMed: 18499668]
48. Wei G, de Leeuw E, Pazgier M, Yuan W, Zou G, Wang J, Ericksen B, Lu WY, Lehrer RI, Lu W. Through the looking glass, mechanistic insights from enantiomeric human defensins. J Biol Chem. 2009; 284:29180–29192. [PubMed: 19640840]
49. Thomassin JL, Lee MJ, Brannon JR, Sheppard DC, Gruenheid S, Le Moual H. Both group 4 capsule and lipopolysaccharide O-antigen contribute to enteropathogenic *Escherichia coli* resistance to human α-defensin 5. PLoS One. 2013; 8:e82475. [PubMed: 24324796]
50. Moser S, Chileveru HR, Nolan EM, Tomaras J. A Bacterial Mutant Library as a Tool to Study the Attack of a Defensin Peptide. Chembiochem. 2014; 15:2684–2688. [PubMed: 25430675]
51. Schmidt NW, Mishra A, Lai GH, Davis M, Sanders LK, Tran D, Garcia A, Tai KP, McCray PB, Ouellette AJ, Selsted ME, Wong GCL. Criterion for amino acid composition of defensins and antimicrobial peptides based on geometry of membrane destabilization. J Am Chem Soc. 2011; 133:6720–6727. [PubMed: 21473577]
52. Van den Bogaart G, Guzmán JV, Mika JT, Poolman B. On the mechanism of pore formation by melittin. J Biol Chem. 2008; 283:33854–33857. [PubMed: 18819911]

53. Falagas ME, Kasiakou SK. Colistin: the revival of polymyxins for the management of multidrug-resistant Gram-negative bacterial infections. Clin Infect Dis. 2005; 40:1333–1341. [PubMed: 15825037]
54. Sochacki, Ka, Barns, KJ., Bucki, R., Weisshaar, JC. Real-time attack on single *Escherichia coli* cells by the human antimicrobial peptide LL-37. Proc Natl Acad Sci U S A. 2011; 108:E77–81. [PubMed: 21464330]
55. Matsuzaki K, Sugishita K, Harada M, Fujii N, Miyajima K. Interactions of an antimicrobial peptide, magainin 2, with outer and inner membranes of Gram-negative bacteria. Biochim Biophys Acta. 1997; 1327:119–130. [PubMed: 9247173]
56. Spindler EC, Hale JDF, Giddings TH, Hancock REW, Gill RT. Deciphering the mode of action of the synthetic antimicrobial peptide Bac8c. Antimicrob Agents Chemother. 2011; 55:1706–1716. [PubMed: 21282431]
57. Yao Z, Kahne D, Kishony R. Distinct single-cell morphological dynamics under beta-lactam antibiotics. Mol Cell. 2012; 48:705–712. [PubMed: 23103254]
58. Paradis-Bleau C, Kritikos G, Orlova K, Typas A, Bernhardt TG. A genome-wide screen for bacterial envelope biogenesis mutants identifies a novel factor involved in cell wall precursor metabolism. PLoS Genet. 2014; 10:e1004056. [PubMed: 24391520]
59. Yeh YC, Comolli LR, Downing KH, Shapiro L, McAdams HH. The caulobacter Tol-Pal complex is essential for outer membrane integrity and the positioning of a polar localization factor. J Bacteriol. 2010; 192:4847–4858. [PubMed: 20693330]
60. Goldman MJ, Anderson GM, Stolzenberg ED, Kari UP, Zasloff M, Wilson JM. Human beta-defensin-1 is a salt-sensitive antibiotic in lung that is inactivated in cystic fibrosis. Cell. 1997; 88:553–560. [PubMed: 9038346]
61. Zhang Y, Cougnon FBL, Wanniarachchi YA, Hayden JA, Nolan EM. Reduction of human defensin 5 affords a high-affinity zinc-chelating peptide. ACS Chem Biol. 2013; 8:1907–1911. [PubMed: 23841778]
62. Chung HS, Yao Z, Goehring NW, Kishony R, Beckwith J, Kahne D. Rapid beta-lactam-induced lysis requires successful assembly of the cell division machinery. Proc Natl Acad Sci U S A. 2009; 106:21872–21877. [PubMed: 19995973]
63. Kulp A, Kuehn MJ. Biological functions and biogenesis of secreted bacterial outer membrane vesicles. Annu Rev Microbiol. 2010; 64:163–184. [PubMed: 20825345]
64. Nguyen T, Francis MB. Practical synthetic route to functionalized rhodamine dyes. Org Lett. 2003; 5:3245–3248. [PubMed: 12943398]
65. Park CB, Yi KS, Matsuzaki K, Kim MS, Kim SC. Structure-activity analysis of buforin II, a histone H2A-derived antimicrobial peptide: the proline hinge is responsible for the cell-penetrating ability of buforin II. Proc Natl Acad Sci U S A. 2000; 97:8245–8250. [PubMed: 10890923]
66. Barns KJ, Weisshaar JC. Real-time attack of LL-37 on single *Bacillus subtilis* cells. Biochim Biophys Acta. 2013; 1828:1511–1520. [PubMed: 23454084]
67. Ding B, Soblosky L, Nguyen K, Geng J, Yu X, Ramamoorthy A, Chen Z. Physiologically-relevant modes of membrane interactions by the human antimicrobial peptide, LL-37, revealed by SFG experiments. Sci Rep. 2013; 3:1854. [PubMed: 23676762]
68. Bindman NA, van der Donk WA. A general method for fluorescent labeling of the N-termini of lanthipeptides and its application to visualize their cellular localization. J Am Chem Soc. 2013; 135:10362–10371. [PubMed: 23789944]
69. Oliver PM, Crooks JA, Leidl M, Yoon EJ, Saghatelian A, Weibel DB. Localization of Anionic Phospholipids in *Escherichia coli* Cells. J Bacteriol. 2014; 196:3386–3398. [PubMed: 25002539]

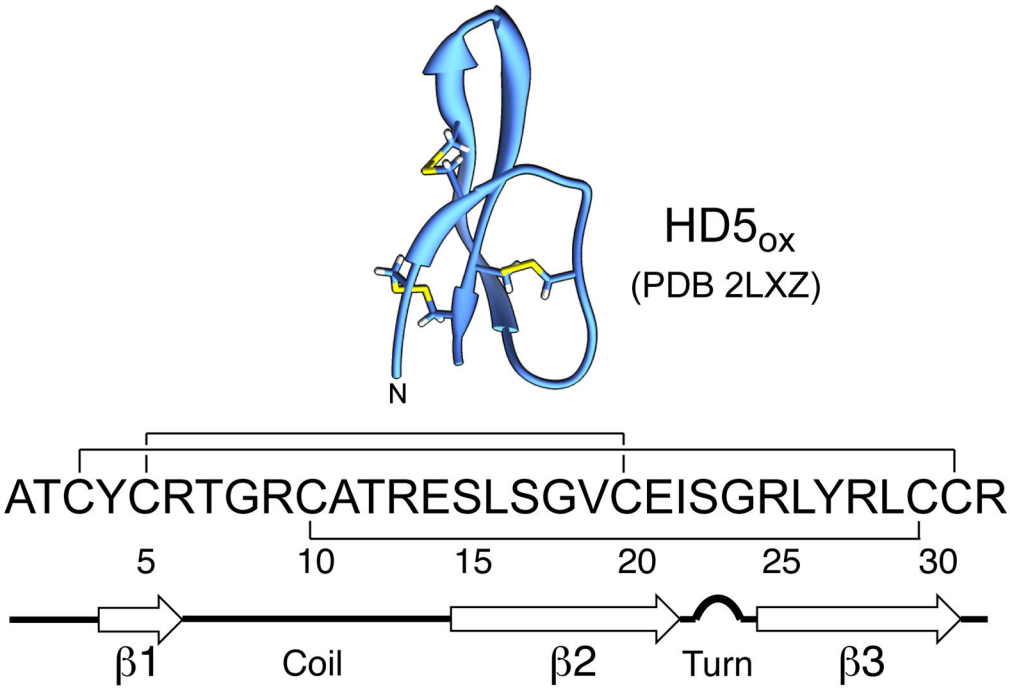

Figure 1.

Structure of the $HD5_{ox}$ monomer determined by solution NMR (PDB 2LXZ)[19] and amino acid sequence. The regiospecific disulfide bond linkages and secondary structure are indicated.

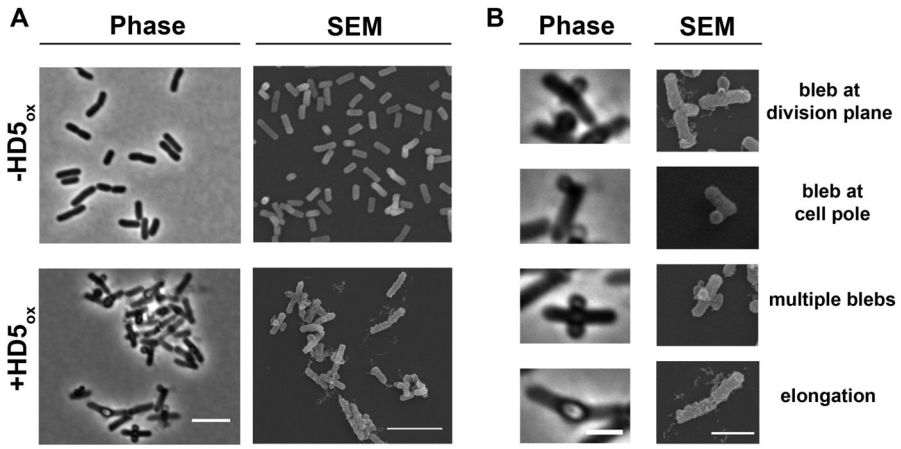

Figure 2.

$HD5_{ox}$ causes distinct morphological changes in *E. coli* that include bleb formation, cellular elongation, and clumping. (A) Phase-contrast and the SEM images of *E. coli* ATCC 25922 (1×10^8 CFU/mL) in the absence ($-HD5_{ox}$) or presence ($+HD5_{ox}$) of 20 μM $HD5_{ox}$, scale = 5 μm. (B) Phase-contrast and the SEM images of single cells illustrate the various morphologies caused by $HD5_{ox}$, scale = 2 μm.

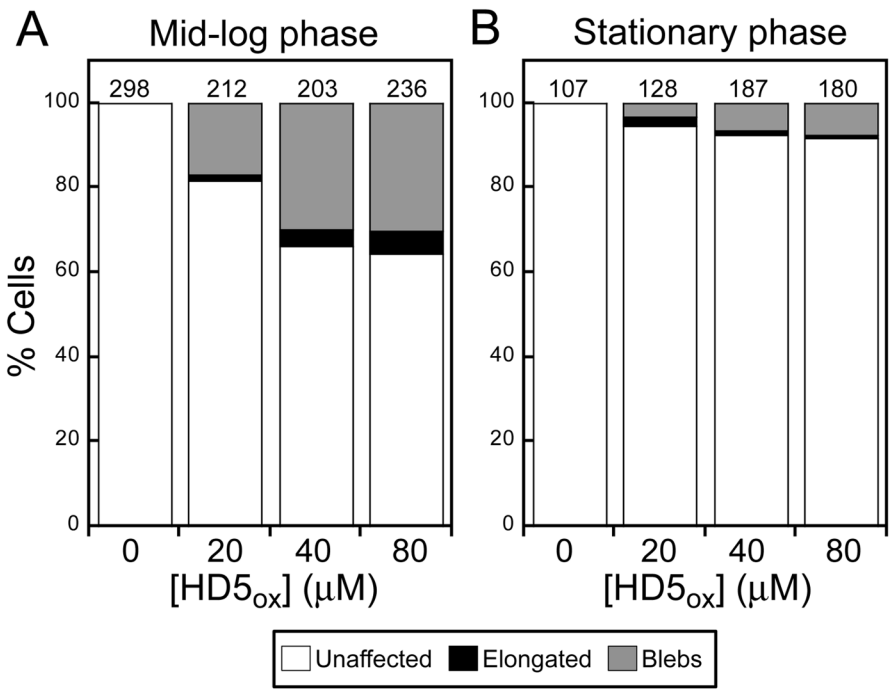

Figure 3.

Effect of $HD5_{ox}$ treatment on *E. coli* ATCC 25922 morphology. The cells (1×10^8 CFU/mL) were treated with varying concentrations of $HD5_{ox}$ for 1 h at 37 °C (10 mM sodium phosphate buffer, pH 7.4, 1% (v/v) TSB). (A) Quantification of unaffected as well as elongated and bleb morphologies for mid-log phase *E. coli*. (B) Quantification for stationary-phase *E. coli*. The number above each bar indicates the number of cells counted.

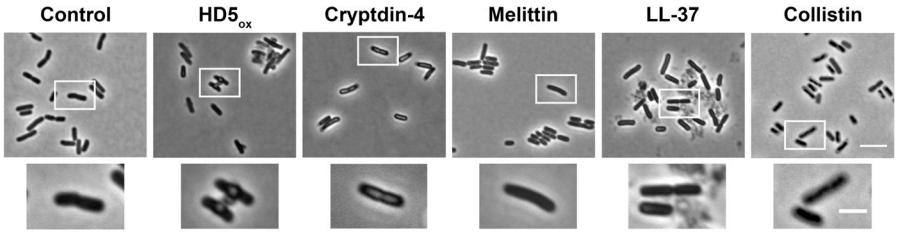

Figure 4.

The consequences of various antimicrobial peptides on *E. coli* morphology. *E. coli* ATCC 29522 (1×10^8 CFU/mL, mid-log phase) were exposed to each peptide (20 μM) for 1 h at 37 °C (10 mM sodium phosphate buffer, pH 7.4, 1% (v/v) TSB) prior to imaging. Top panels, scale = 5 μm; bottom panels, scale = 2 μm.

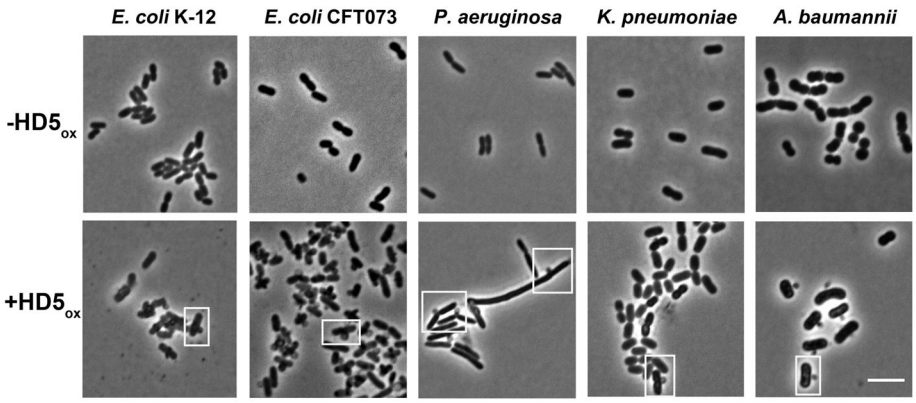

Figure 5.

The effect of $HD5_{ox}$ exposure on the morphology of Gram-negative bacteria. Each microbe (1×10^8 CFU/mL, mid-log phase) was exposed to $HD5_{ox}$ (20 μM except for *P.* aeruginosa where 40 μM was used) for 1 h at 37 °C (10 mM sodium phosphate buffer, pH 7.4, 1% v/v TSB) prior to imaging. Scale = 5 μm. Additional images are provided in Figure S6.

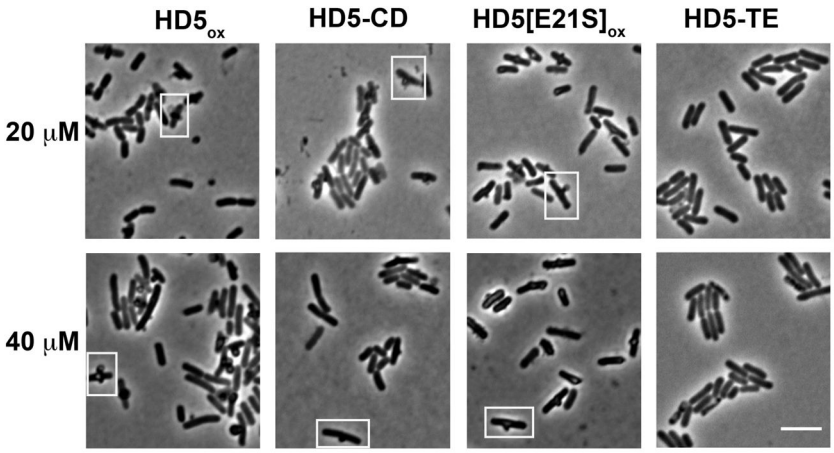

Figure 6.

E. coli morphologies in the presence of HD5 derivatives reveal that the disulfide bonds are necessary for bleb formation. *E. coli* ATCC 25922 (1×10^8 CFU/mL, mid-log phase) was exposed to each peptide for 1 h at 37 °C (10 mM sodium phosphate buffer, pH 7.4, 1% v/v TSB) prior to imaging. Scale = 5 μm.

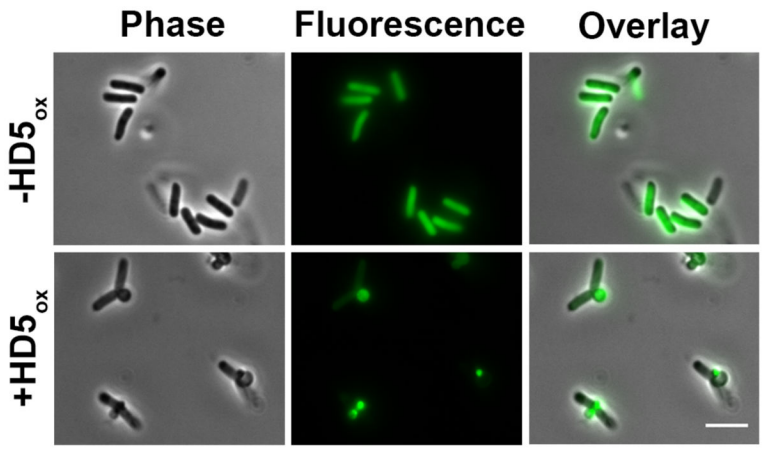

Figure 7.

Treatment of *E. coli* cyto-GFP with $HD5_{ox}$ reveals that the cytoplasmic contents leak into the blebs. *E. coli* cyto-GFP (1×10^7 CFU/mL, mid-log phase) were exposed to 4 μM $HD5_{ox}$ for 1 h at 37 °C (10 mM sodium phosphate buffer, pH 7.4, 1% v/v TSB) prior to imaging. Scale = 5 μm.

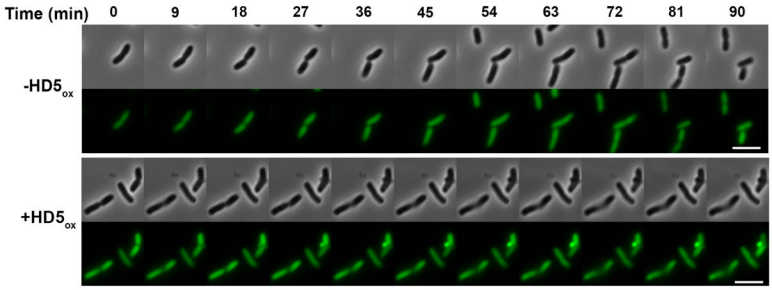

Figure 8.

Time-lapse imaging of *E. coli* cyto-GFP (1×10^7 CFU/mL, mid-log phase) treated with 20 μM $HD5_{ox}$ with $HD5_{ox}$ at 37 °C (10 mM sodium phosphate buffer, pH 7.4, 1% v/v TSB). Scale = 5 μm.

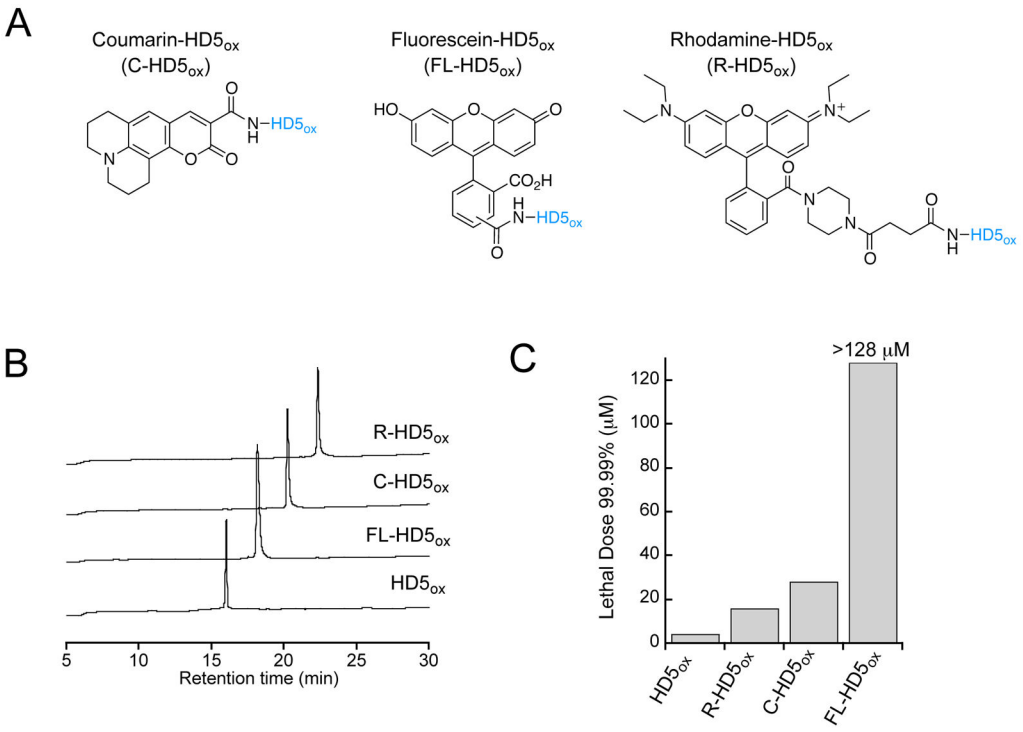

Figure 9.

Functionalization of the $HD5_{ox}$ N-terminus affords three fluorophore-$HD5_{ox}$ conjugates. (A) Structures of coumarin-, fluorescein-, and rhodamine-derivatized $HD5_{ox}$. The $HD5_{ox}$ primary sequence is presented in Figure 1. (B) Analytical HPLC traces (220 nm absorption, 10–60% B over 30 min, 1 mL/min) of purified peptides. (C) Antimicrobial activity of the peptides against *E. coli* ATCC 25922 (n = 3).

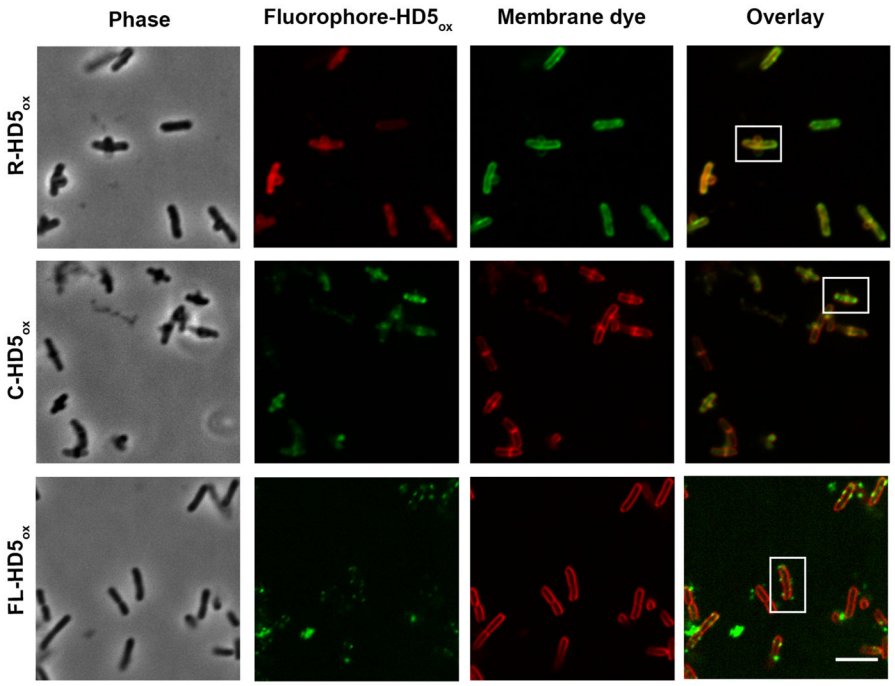

Figure 10.

Fluorescence imaging of *E. coli* treated with fluorophore-$HD5_{ox}$ conjugates and membrane dyes. *E. coli* ATCC 25922 (1×10^8 CFU/mL, mid-log phase) treated with R-$HD5_{ox}$ (20 μM), C-$HD5_{ox}$ (20 μM), and FL-$HD5_{ox}$ (8 μM) at 37 °C (10 mM sodium phosphate buffer, pH 7.4, 1% v/v TSB) and incubated with 2 μg/mL of FM1-43 for R-$HD5_{ox}$ sample and 2 μg/mL of FM 4–64 for both C-$HD5_{ox}$ and FL-$HD5_{ox}$ samples prior to imaging. The boxed cells are depicted in Figure 11. Scale = 5 μm.

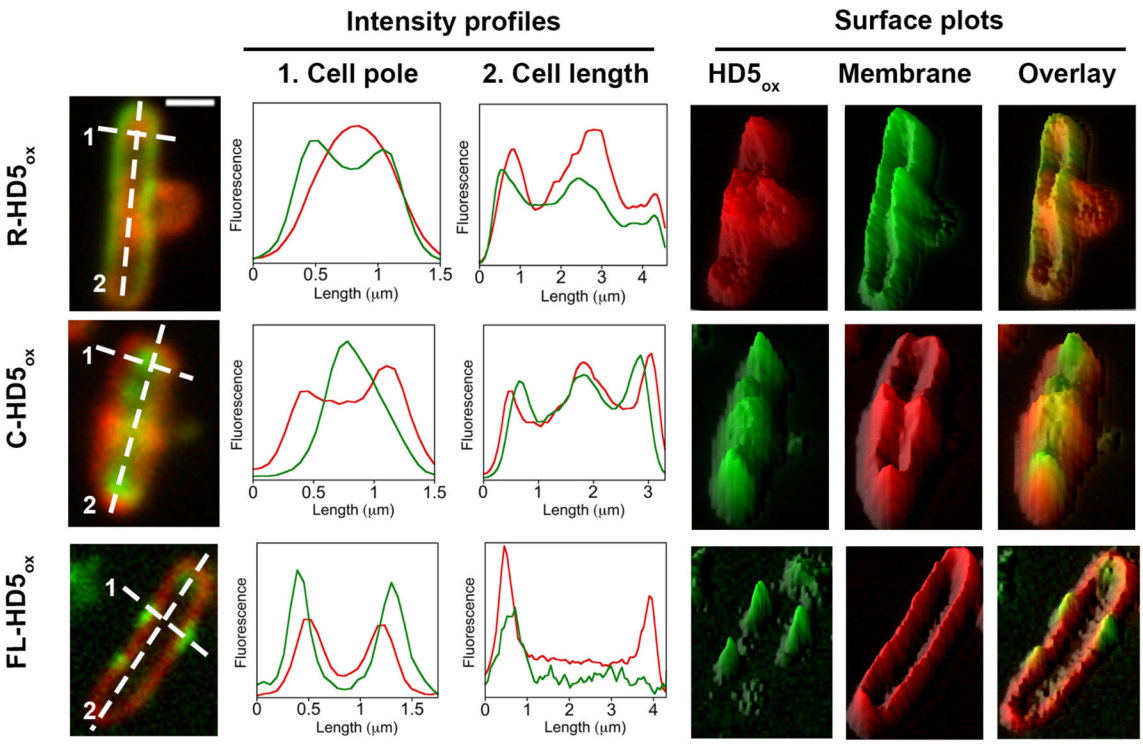

Figure 11.

Intensity profiles and surface plots of the boxed cells depicted in Figure 10. Fluorescence intensities along the cell poles (dashed line 1) and across cell (dashed line 2) are plotted. Surface plots were generated using ImageJ software. Scale = 1 μm.